# Renal IL-23–Dependent Type 3 Innate Lymphoid Cells Link Crystal-induced Intrarenal Inflammasome Activation with Kidney Fibrosis

**Teresa M. Frasconi,*[,1,2] Christian Kurts,*[,†,1] Ermanila Dhana,* Romina Kaiser,* Miriam Reichelt,* Veronika Lukacs-Kornek,* Peter Boor,[‡] Anja E. Hauser,[§,¶] Anna Pascual-Reguant,[§,¶] Sammy Bedoui,[†] Jan-Eric Turner,[‖] Janine Becker-Gotot,*[,3] and Isis Ludwig-Portugall*[,3,4]**

**Chronic inflammasome activation in mononuclear phagocytes (MNPs) promotes fibrosis in various tissues, including the kidney. The cellular and molecular links between the inflammasome and fibrosis are unclear. To address this question, we fed mice lacking various immunological mediators an adenine-enriched diet, which causes crystal precipitation in renal tubules, crystal-induced inflammasome activation, and renal fibrosis. We found that kidney fibrosis depended on an intrarenal inflammasome-dependent type 3 immune response driven by its signature transcription factor Rorc (retinoic acid receptor-related orphan receptor C gene), which was partially carried out by type 3 innate lymphoid cells (ILC3s). The role of ILCs in the kidney is less well known than in other organs, especially that of ILC3. In this article, we describe that depletion of ILCs or genetic deficiency for Rorc attenuated kidney inflammation and fibrosis. Among the inflammasome-derived cytokines, only IL-1β expanded ILC3 and promoted fibrosis, whereas IL-18 caused differentiation of NKp46$^+$ ILC3. Deficiency of the type 3 maintenance cytokine, IL-23, was more protective than IL-1β inhibition, which may be explained by the downregulation of the IL-1R, but not of the IL-23R, by ILC3 early in the disease, allowing persistent sensing of IL-23. Mechanistically, ILC3s colocalized with renal MNPs in vivo as shown by multiepitope-ligand cartography. Cell culture experiments indicated that renal ILC3s caused renal MNPs to increase TGF-β production that stimulated fibroblasts to produce collagen. We conclude that ILC3s link inflammasome activation with kidney inflammation and fibrosis and are regulated by IL-1β and IL-23.** ***The Journal of Immunology*****, 2024, 213: 865–875.**

Crystal-induced inflammasome activation drives inflammation and fibrosis in various diseases and organs, including arteriosclerosis, gout, Alzheimer's disease, liver fibrosis, and silica- or asbestos-induced lung fibrosis (1–5). The urine concentration and acidification function of the kidney favors intratubular crystal formation, when the solubility coefficient of metabolites is exceeded (6, 7). Crystals may cause kidney disease by obstructing renal tubules, but recent work uncovered that they may also promote inflammasome activation in renal mononuclear phagocytes (MNPs) (7–11). These include dendritic cells and macrophages, and play important roles in kidney homeostasis, defense against infections, and in sterile nephritis (12–15). They were also shown to phagocytose crystals, which evokes the activation of the NACHT, LRR, and PYD domain-containing protein 3 (NLRP3)-dependent inflammasome that produces IL-1β and IL-18. The important role of these cytokines in crystal-induced nephritis has been demonstrated in knockout (KO) mice lacking them, their receptors, or NLRP3 (8, 16), and in experiments where pharmacological inhibitors of these mediators were administered (17). Also, in models of primary hyperoxaluria and 2,8 dihydroxy-adenine urolithiasis, these maneuvers lowered local and systemic IL-1β and IL-18 levels and reduced kidney fibrosis (18).

In recent years, innate lymphoid cells (ILCs) have gained much attention in inflammatory diseases (19–22). ILCs are a family of

*Institute of Molecular Medicine and Experimental Immunology, University Hospital Bonn, Bonn, Germany; [†]Department of Microbiology and Immunology, Doherty Institute for Infection and Immunity, University of Melbourne, Melbourne, Victoria, Australia; [‡]Institute of Pathology, Department of Nephrology, RWTH University, Aachen, Germany; [§]Department of Rheumatology and Clinical Immunology, Charité–Universitätsmedizin Berlin, corporate member of Freie Universität Berlin and Humboldt-Universität zu Berlin, Berlin, Germany; [¶]Immune Dynamics, Deutsches Rheuma-Forschungszentrum, Leibniz Institute, Berlin, Germany; and [‖]III Department of Medicine, University Medical Center Hamburg-Eppendorf, Hamburg, Germany

[1]T.M.F. and C.K. contributed equally as cofirst authors.

[2]Current address: Molecular Partners, Zurich, Switzerland.

[3]J.B.-G. and I.L.-P. contributed equally as cosenior authors.

[4]Current address: Miltenyi Biotec B.V. & CO. KG, Teterow Branch, Teterow, Germany.

ORCIDs: 0000-0002-6620-2401 (C.K.); 0009-0007-1639-7953 (E.D.); 0009-0000-4906-5540 (R.K.); 0000-0001-9921-4284 (P.B.); 0000-0002-7725-9526 (A.E.H.); 0000-0002-5042-3699 (A.P.-R.); 0000-0003-1190-2133 (J.B.-G.); 0000-0002-9463-7111 (I.L.-P.).

Received for publication January 26, 2024. Accepted for publication July 5, 2024.

This work was supported by the German Research Foundation (Deutsche Forschungsgemeinschaft [DFG]) (Grants "SFB/TRR57" 36842431, "SPP1937" 273942223, "SFB1192" 264599542, "IRTG2168" 272482170, "SFB1454" 432325352, "KFO329" 386793560, and "FOR5427" 466687329; individual DFG Grants 322900939, 454024652, 432698239, 445703531, and TU-316/1-3), and Germany's Excellence Strategy (Grant "EXC 2151" 390873048), and by the European Research Council (Grant "101001791") under Horizon 2020 program.

I.L.-P., J.B.-G., and C.K. conceptualized the study. T.M.F. performed the experiments with R.K., J.B.-G., and M.R. P.B. performed the histological stainings and analysis. E.D. and J.B.-G. performed the in vitro assays. A.P.-R. and A.E.H. performed the multiepitope-ligand cartography analysis of the kidney sections. J.-E.T. provided mice and expertise for innate lymphoid cell analysis, V.L.-K. for fibroblasts, and S.B. for T cell analysis. I.L.-P., J.B.-G., C.K., and T.M.F. discussed data and wrote the manuscript. All authors discussed and interpreted the data.

Address correspondence and reprint requests to Dr. Isis Ludwig-Portugall and Dr. Janine Becker-Gotot, Biomedical Center II, University Clinic, University of Bonn, Venusberg Campus 1, 53127 Bonn, Germany. E-mail addresses: isisl@miltenyi.com (I.L.-P.) and jbecker-gotot@uni-bonn.de (J.B.-G.)

The online version of this article contains supplemental material.

Abbreviations used in this article: ILC, innate lymphoid cell; KO, knockout; MFI, mean fluorescence intensity; MNP, mononuclear phagocyte; NLRP3, NACHT, LRR, and PYD domain-containing protein 3; Rorc, RAR-related orphan receptor C gene; Rorγt, RAR-related orphan receptor γt; α-SMA, α-smooth muscle actin; WT, wild-type.



https://doi.org/10.4049/jimmunol.2400041

leukocytes with lymphoid morphology that lack Ag-specific receptors and arise in the bone marrow from the common lymphoid progenitor (23, 24). The current classification includes NK cells and three subsets of ILCs, termed type 1 ILC (ILC1), type 2 ILC (ILC2), and type 3 ILC (ILC3) (25–27). ILC1s express the transcription factor T-bet, are activated by IL-12, and produce IFN-γ upon activation (28, 29). ILC2s express the transcription factor GATA-3, are induced by IL-4, IL-25, and IL-33, and release IL-4, IL-5, and IL-13 (30). ILC3s express the transcription factor RAR-related orphan receptor γt (Rorγt), are maintained by IL-23 (31–33), and produce IL-17, IL-22 and GM-CSF (34–36). Other cells capable of producing type 3 cytokines include Th17 cells, γδ T cells, and mucosal-associated invariant T cells (37, 38). These cytokines promoted glomerulonephritis (39), but their role in inflammasome-mediated nephritis is not yet fully understood (40, 41).

ILCs have been detected in several organs, especially in barrier organs, such as the lung, the intestine, and the skin, but also in the kidney (42–44). As tissue-resident cells, they are thought to act as sentinels against bacterial, viral, and parasitic infections (45, 46). However, they may also contribute to autoimmune or chronic inflammatory diseases (47), for example, in the liver, lung, and intestine (48). ILCs are activated by environmental stimuli and then produce cytokines locally (49). Stimuli include alarmins released in the context of tissue damage or from resident immune cells, such as macrophages.

Recently, different ILC populations were identified within the kidney, and their role in nephritis was investigated (50, 51). A rare population of ILC2s has been described that promoted IL-33–dependent repair in Adriamycin-induced murine glomerulosclerosis (43, 52, 53). ILC3s have very recently been described to aggravate adaptive immunity in a model of lupus nephritis (54) and to aggravate fibrosis resulting from unilateral ureteral obstruction (55), but a role in inflammasome-dependent kidney inflammation has not been described yet. In this study, we investigated the immune mechanism underlying crystal-induced, inflammasome-mediated kidney fibrosis (56). We detected increasing numbers of intrarenal ILC3s in response to IL-1β and demonstrate that they mechanistically link inflammasome activation with kidney fibrosis.

## Materials and Methods

### *Mice and model of crystal-induced kidney fibrosis*

C57BL/6J, Rag2 KO, Rorc (RAR-related orphan receptor C gene) KO (57), IL-18R KO (58), IL-1R KO, IL-17A KO (59), IL-22 KO (60), and IL-23p19 KO (61) mice between 8 and 12 wk of age were bred in the animal facility of the University Clinic of Bonn. To induce crystal nephritis, we fed female or male littermate mice 14 or 21 d with 0.2% adenine-enriched diet, as described previously (18). Thy1.2$^+$ cells were depleted with anti-murine Thy1.2 Ab (BioXCell). IL-1β was neutralized with anti-murine IL-1β Ab. IL-1β was neutralized by injecting 45 μg/mouse of anti-murine IL-1β Ab (BioXCell) i.p. on days 1, 4, 7, and 10 of adenine-enriched diet. All animal experiments were approved by German state government authorities (LANUV, Düsseldorf, Germany).

### *Murine cell isolation and restimulation ex vivo*

Kidneys of mice were excised, cut into pieces, and digested in RPMI medium enriched with 2% FCS, 1% penicillin-streptomycin (Pen/Strep), DNase (0.1 mg/ml), and Collagenase (1 mg/ml) as described previously (62). The cell suspension was filtered, washed, and incubated for 4 h at 37°C in RPMI medium enriched with 10% FCS, 1% Pen/Strep, 1% 2-ME, 20 ng/ml rmIL-7 (PeproTech), 1 μg/ml Ionomycin (Sigma-Aldrich), 0.5 μg/ml PMA (Sigma-Aldrich), and brefeldin A (GolgiPlug) (eBioscience) 1:1000 diluted. After restimulation, cells were washed and stained.

### *Isolation of ILC precursors, ILC3 differentiation, and enrichment*

Kidneys were digested and homogenized, RBCs were lysed, and lineage$^-$ cells were enriched as described earlier (Miltenyi). Thy1.1$^+$ ILC precursor cells were isolated using a kit (Miltenyi), and $5 \times 10^4$ were incubated for 10 d in a 96-well plate at 37°C and 5% $CO_2$. Cells were resuspended in 200 μl of X-Vivo medium supplemented with IL-2 (25 ng/ml; PeproTech), IL-7 (25 ng/ml; PeproTech), SCF (25 ng/ml; PeproTech), IL-23 (10 ng/ml; Miltenyi), IL-1β (10 ng/ml; PeproTech), IL-18 (10 ng/ml; R&D Systems), and TGF-b (2 ng/ml; PeproTech). Medium was changed every other day. ILC3s were enriched for MNP-coculture experiments by MACS-based depletion of ILC1s and ILC2s using NK1.1-bio (BD) or ST2-bio (BD) and streptavidin beads, respectively. ILC3 differentiation was verified by FACS.

### *Fibroblast culture*

Primary skin fibroblasts were purified from ears of C57BL/6 mice, in passage 3 seeded into 96-well plates and cocultured with purified CD11c$^+$ renal MNPs isolated using a kit (Miltenyi). In brief, ears were digested in FCS-free RPMI medium containing DNAse I (0.1 mg/ml; Roche) and Collagenase P (0.2 mg/ml; Roche) for 2–3 h. Cells were collected, counted, and plated in a six-well plate at a concentration of $5 \times 10^5$ cells/2 ml in RPMI media containing 10% FCS + 1% Pen/Strep per well. On the next day, unattached cells were removed and wells were washed with PBS. Medium was exchanged on day 2, and cells were split and passaged when confluent. Fibroblasts were then seeded into 96-well plates and used in the fibroblast coculture assays with renal MNPs.

### *Abs and flow cytometry analysis*

Surface molecules were stained with CD45-PerCpCy5.5 or CD45-BV421 (30F11), NKp46-BV510 (29A1.4), Thy1.2-PE, Thy1.2-BV510, or Thy1.2-PECy7 (53-2.1) from BioLegend. IL-18R-PE (P3TUNYA) was from eBioscience, and IL-1R-Alexa 647 (JAMA147) from Bio-Rad. For the lineage mixture, these biotinylated Abs from eBioscience were combined: Ly6G (RB6-8C5) and CD5 (53-7.3). The following Abs were from Invitrogen: CD11c (N418), γδ TCR (UC7-13D5), CD19 (MB19-1), CD11b (M1/70), and CD3ε (145-2C11). TCRβ (H57-597) was from BioLegend. Renal lymphocytes were gated as CD45$^+$Thy1.2$^+$ cells and identified as lineage$^-$ using the earlier-described lineage mixture to define ILCs except in Supplemental Fig. 6, where we stained separately for γδ TCR to identify (1) Thy1.2$^+$lineage$^+$γδ TCR$^-$αβTCR$^+$ lymphocytes, (2) Thy1.2$^+$lineage$^+$γδ TCR$^+$ lymphocytes, and (3) Thy1.2$^+$lineage$^-$γδ TCR$^-$ innate ILCs. The total cell number was calculated by using absolute counting beads (ThermoFisher) with the formula: ([no. of events acquired × no. of beads added in the sample]/no. of beads acquired) × fraction of kidney volume used for staining. ILC1s were identified as CD45$^+$Thy1.2$^+$lineage$^-$αβTCR$^-$γδ TCR$^-$ T-bet$^+$ cells, ILC2s as CD45$^+$Thy1.2$^+$lineage$^-$αβTCR$^-$γδ TCR$^-$GATA3$^+$, and ILC3s as CD45$^+$Thy1.2$^+$lineage$^-$αβTCR$^-$γδ TCR$^-$Rorγt$^+$. After staining with the mixture, Abs were labeled with fluorochrome-labeled streptavidin conjugates (BioLegend). For intracellular staining, surface molecules were stained first, cells were fixed and permeabilized with a kit (eBioscience), then stained with GATA3-Alexa 647 (L50-823; BD Biosciences), IFN-γ-FITC, or IFN-γ-allophycocyanin (XMG1.2), IL-17A-BV421 (TC11-18H10.1), T-bet-BV421 (4B10), Rorγ-Alexa 647 (Q31-378), or Ki67-PE/Cyanine7 (11F6) from BioLegend or Rorγ-Pacific Blue (Q31-378) or Eomes-Alexa 488 (X4-83) from BD Biosciences. Dead cells were excluded by using a fixable viability dye (Invitrogen). Data were acquired with a BD Canto II and analyzed with FlowJo (Tree Star).

### *Measurement of soluble factors*

The IFN-γ, IL-17A, and TNF-α production of sorted living, CD45$^+$Lin$^-$, Thy1.2$^+$ ILCs were determined by Luminex assay according to the manufacturer's instructions (Affymetrix). In short, sorted ILCs were plated in 40 μl/well into a 96-well plate and restimulated by PMA (500 ng/ml) and Ionomycin (1 μg/ml) overnight. Culture supernatants were measured by Bio-Rad BioPlex analyzer (Bio-Rad).

### *Multiplexed cytometric bead assay*

Lineage$^-$, Thy1.2$^+$, Rorγt$^+$, or Rorγt$^-$ ILCs were sorted using Rorc reporter mice using a BD Aria and plated into a 96-well plate and were restimulated by PMA (500 ng/ml) and Ionomycin (1 μg/ml) overnight. Culture supernatants were collected and measured by LEGENDplex Mouse Inflammation panel according to the manufacturer's instructions and analyzed by software from BioLegend.

### *Histology*

Tissues were fixed in methyl Carnoy's solution, paraffin embedded, and cut into 1-μm sections. Periodic acid–Schiff staining was used to assess renal morphology. Collagen type III (Southern Biotechnology Associates) and α-smooth muscle actin (α-SMA; Dako) staining were performed as described previously (16, 63). For negative controls, isotype-matched IgG

was used, and no unspecific staining was observed. Whole slides were digitalized using a whole-slide scanner NanoZoomer 2.0-HT and analyzed using NDP.view (Hamamatsu Photonics) and ImageJ (NIH) software. The percentage of stained area was analyzed in 16–22 consecutive fields omitting larger vessels at ×20 magnification, representing almost the entire kidney area. All analyses were performed in a blinded manner.

### *Multiepitope-ligand cartography*

Multiepitope-ligand cartography was performed as described previously (64). In brief, 4% PFA-fixed kidney sections were cut in 5-μm sections with a MH560 cryotome (ThermoFisher) on 3-aminopropyltriethoxysilane–coated cover slides (24 × 60 mm; Menzel-Gläser). Samples were rehydrated, blocked, and permeabilized with 0.2% Triton X-100 in PBS for 10 min at room temperature, and unspecific binding was blocked with 10% goat serum and 1% BSA in PBS for at least 20 min. A fluid chamber was created with "press-to-seal" silicone sheets (1.0 mm thickness; Life Technologies) with a circular cutout (10-mm diameter), which was attached to the coverslip surrounding the sample holding 100 μl of PBS. The tissue section was then incubated with PE, allophycocyanin, or FITC-coupled Abs (anti-B220, anti-CD5, anti-Gr1, anti-FcER1a, anti-CD45, anti-CD90.2, anti-CD127, anti-Rorγt, anti-CD11b, anti-F4/80, anti-CD3, anti-CD31, and DAPI). A fluorescence image was taken with three fluorescence channels acquired in parallel in one cycle, followed by repetitive washing steps. Afterward, a phase-contrast image was taken to adjust the autofocus and to ensure a stable image focus between imaging cycles. After image acquisition, the fluorescence was bleached by light exposure and a bleaching control image was taken. All steps were performed in an automated system, using a pipetting robot and a Leica microscope (Toponome Imaging Cycler). To analyze the multiplexed imaging data and computationally identify ILCs, T cells, and MNPs, we used an automated analysis pipeline in CellProfiler that segments single cells within images and measures mean fluorescence intensities (MFIs) of all markers included in the experiment for each cell (65). With this single-cell information, cell types can be identified based on thresholding of MFI for relevant markers. ILCs were defined as cells with MFI RORγt > 0.2, MFI CD3 < 0.04, MFI B220 < 0.05, MFI Gr1 < 0.02, and FcεR1a < 0.05. T cells were defined as cells with MFI CD45 > 0.1 and MFI CD3 > 0.1. We defined MNPs as cells with MFI CD11b > 0.07 and MFI F4/80 > 0.12. The area within a 10-μm radius (corresponding to the average diameter of a hematopoietic cell) around each ILC was defined as the ILC neighborhood or niche, and the distribution of MNP and T cells in this area was quantified. The same neighborhood analysis was performed for T cells with respect to MNP.

### *Statistics*

Results are expressed as mean ± SEM if not otherwise stated. The statistical analysis to compare three or more groups was performed with one-way ANOVA with Tukey posttest; Mann–Whitney was performed to compare two groups. Data were analyzed with GraphPad Prism version 10.

## Results

### *ILC1 and ILC3 are increased during inflammasome-mediated nephritis*

To study how inflammasome-mediated inflammation causes kidney fibrosis, we fed mice an adenine-enriched diet for 14 or 21 d (18, 66), which induces the formation of intratubular crystals. These activate the inflammasome in renal MNP, which causes progressive inflammation and eventually kidney fibrosis (8, 16, 17). When we investigated the immune cell infiltrate in the inflamed kidney by flow cytometry on day 14 of the diet (gating scheme in Fig. 1A), we observed an increase in CD45$^+$Thy1.2$^+$lineage$^-$ γδ TCR$^-$ immune cells (Fig. 1B), indicating an accumulation of ILCs. Staining for transcription factors revealed an increase of Tbet$^+$ ILC1s and Rorγt$^+$ ILC3s, but not of GATA3$^+$ ILC2s (Fig. 1C–E), which was unexpected because usually ILC2s are associated with fibrogenic processes (43). EOMES$^+$ NK cells were also unaltered (Supplemental Fig. 1). The accumulation of Rorγt$^+$ ILC3 was dependent on proliferation, as evidenced by Ki67 expression (Supplemental Fig. 2). The Rorγt$^+$ ILCs produced the prototypical type 3 immunity cytokine IL-17A and the Rorγt$^-$ ILCs secreted the type 1 immunity signature cytokine IFN-γ, but only little of the type 2 cytokines IL-4, IL-5, and IL-13 (Fig. 1F–H, Supplemental Fig. 3). These findings identified an accumulation of ILC1 and ILC3 in inflammasome-mediated nephritis.

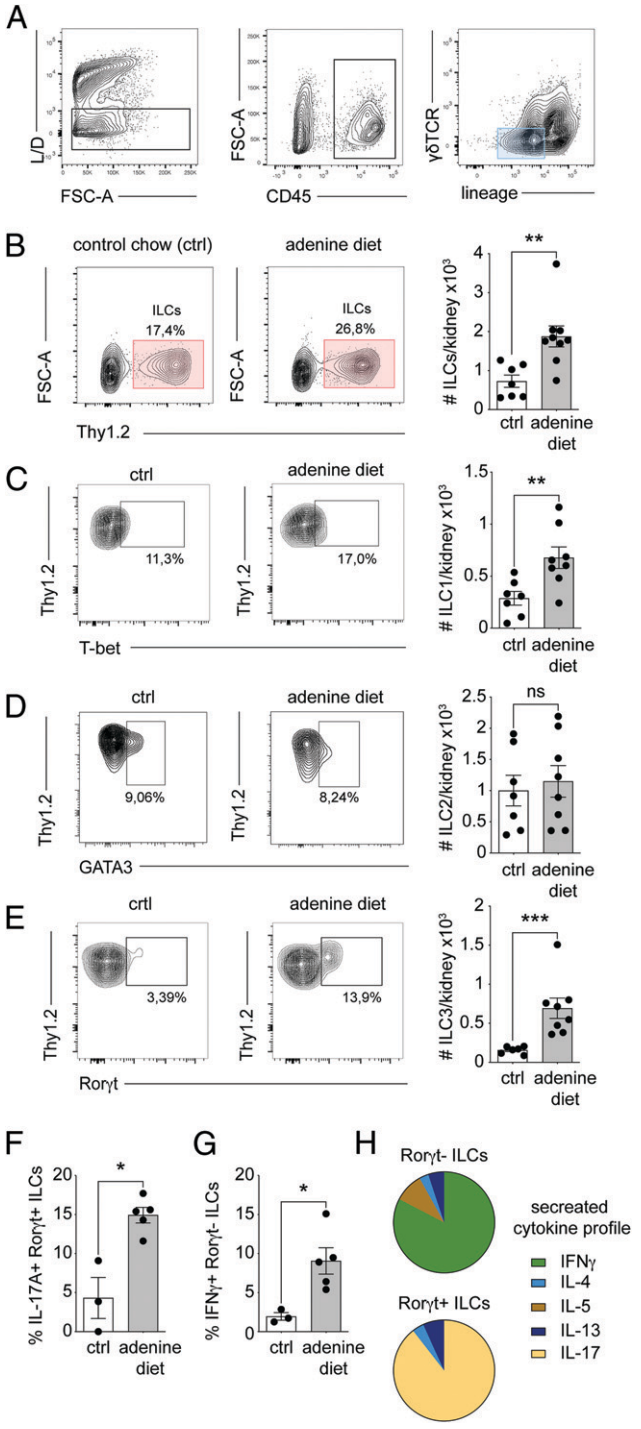


**FIGURE 1.** ILC1 and ILC3 are increased during inflammasome-mediated nephritis. WT mice were fed either with control (ctrl) chow or adenine-enriched diet for 14 d to induce crystal-mediated kidney fibrosis. (**A**) Flow cytometry gating strategy to identify innate lymphocytes in the kidney. Lineage exclusion comprises CD3ε, CD5, αβ-TCR, CD19, Ly6G, CD11c, and CD11b. (**B**–**E**) Identification and quantification of absolute ILCs numbers (B), renal ILC1 (lineage$^-$Thy1.2$^+$T-bet$^+$) (C), ILC2 (lineage$^-$Thy1.2$^+$ GATA3$^+$) (D), and ILC3 (lineage$^-$Thy1.2$^+$Rorγt$^+$) (E). Statistics were calculated using an unpaired Mann–Whitney *U* test ($n$ = 7–8 mice/group), $^*p < 0.05$, $^{**}p < 0.01$, $^{***}p < 0.001$. Data were pooled from two independent experiments and displayed as mean ± SEM. (**F**) Percentage of IL-17A–producing Rorγt$^+$ ILCs or (**G**) IFN-γ–producing Rorγt$^-$ ILCs. (**H**) Cytokine profile of sorted Rorγt$^+$ and Rorγt$^-$ ILCs from five WT mice on adenine-enriched diet. Statistics were calculated using an unpaired Mann–Whitney *U* test ($n$ = 5 mice/group), $^*p < 0.05$. One representative of two independent experiments was shown and depicted as mean ± SEM.

*ILCs promote inflammasome-mediated kidney fibrosis*

To investigate whether ILCs promote inflammasome-mediated kidney fibrosis, we fed the adenine-enriched diet to Rag2 KO mice that harbor ILCs, but no adaptive immune cells, and included an additional group of Rag2 KO mice treated with anti-Thy1.2 Ab to deplete also the ILCs. This strategy is frequently used to perform loss-of-function studies for ILCs (67–69), because no selective depletion method for ILCs exists. Histological analysis revealed that Collagen III and α-SMA deposition in the kidneys of adenine-treated Rag2 KO mice was reduced compared with wild-type (WT) mice (Fig. 2A, 2B), indicating a role for adaptive immune cells in inflammasome-mediated kidney fibrosis. Importantly, anti-Thy1.2 Ab–treated Rag2 KO mice (Rag2KO + anti-Thy1.2) showed an even greater reduction of Collagen III and α-SMA deposition than ILC-competent Rag2 KO (Rag2KO) and WT mice (Fig. 2A, 2B), and also a reduction of serum creatinine compared with WT mice (Fig. 2C) indicative of renal function. These findings confirmed a profibrotic role of ILCs in inflammasome-mediated nephritis.

*IL-1β, and not IL-18, expands intrarenal ILC3 in inflammasome-mediated nephritis and promotes fibrosis*

We next asked how inflammasome activation regulates ILCs during crystal-induced nephritis, focusing on the inflammasome-derived cytokines IL-1β and IL-18 (8). Mice treated with IL-1β blocking Abs or deficient for IL-18R were fed the adenine diet. After 2 wk, we found a significant reduction of intrarenal Rorγt$^+$ ILC3s in anti–IL-1β–treated WT mice compared with WT mice, in contrast with IL-18R KO mice (Fig. 3A), whereas the decrease of IL-17A–producing Rorγt$^+$ ILC3 was not significant (Fig. 3B). Numbers of Rorγt$^-$ ILCs, including ILC1 and ILC2, were unaltered in the absence of either cytokine (Fig. 3C), nor were IFN-γ–producing cells (Fig. 3D). Thus, IL-1β, but not IL-18, selectively expanded ILC3, although we cannot formally exclude that IL-1β acted indirectly on ILC3. Histological analysis of kidney sections of adenine-fed mice showed less α-SMA, but not Collagen III, staining of kidney sections after IL-1β neutralization (Fig. 3E, 3F). To further validate the involvement of IL-1β signaling, we used IL-1R KO mice instead of the blocking Ab, and again noted significantly reduced numbers of ILC3s, but not of Rorγt$^-$ ILCs (Supplemental Fig. 4A, 4B). In this study, deposition of Collagen III was reduced (Supplemental Fig. 2C), but not of α-SMA (Supplemental Fig. 4C). IL-18R KO deficient mice did not show significantly reduced kidney fibrosis parameters (Fig. 3E, 3F). The effects of IL-1β on intrarenal ILC3 numbers and the partial effect on kidney fibrosis endorsed a profibrotic role of ILC3 in our model.

The unchanged ILC3 numbers in IL-18R KO mice (Fig. 3A) did not exclude effects of this cytokine on the phenotype of ILC3. To investigate this possibility, we examined ILC3s isolated from kidneys of WT, IL-18R KO, and as a control, IL-1R KO mice on an adenine-enriched diet. We found that a proportion of renal ILC3s expressed the NK cell marker NKp46 (Supplemental Fig. 5A), which has recently been described to be expressed by ILC3s that responded to environmental stimuli in nonlymphatic tissues (44, 70, 71). NKp46 was increased on ILC3s from WT and on IL-1R KO mice under an adenine-enriched chow, but not on ILC3s from IL-18R KO mice (Supplemental Fig. 5B, 5C). Among the Rorγt$^-$ ILCs, no significant differences in NKp46 expression were seen (Supplemental Fig. 5D, 5E). These findings showed that IL-18, but not IL-1β, promoted the emergence of NKp46$^+$ ILC3, but not of

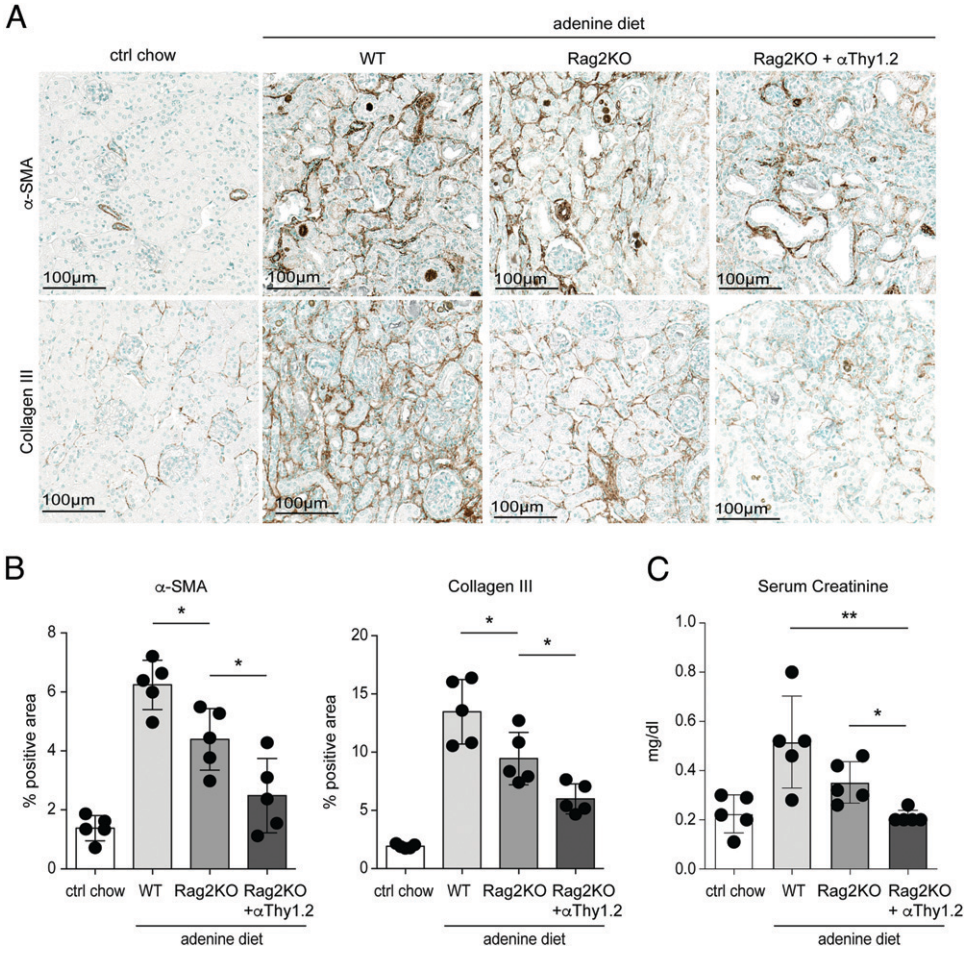


**FIGURE 2.** Innate lymphocytes promote crystal-induced kidney fibrosis. (**A**) α-SMA and Collagen III staining of kidney sections (scale bars, 100 μm) from WT mice on control (ctrl) chow and WT, Rag2 KO mice, and Rag2 KO mice treated with anti-Thy1.2 Ab on adenine-enriched diet for 21 d. Depletion was performed on days −1, 3, 6, 9, and 12 of adenine diet. (**B**) Percentages of α-SMA– and Collagen III–positive areas in kidney sections depicted in (A). (**C**) Serum creatinine levels in the serum of ctrl chow mice, WT mice, and Rag2 KO mice and treated with anti-Thy1.2 Ab on adenine-enriched diet. Statistics were calculated using a one-way ANOVA with Tukey posttest ($n$ = 4–5 mice/group), $^*p < 0.05$, $^{**}p < 0.01$. One representative of two independent experiments was shown and depicted as mean ± SD.

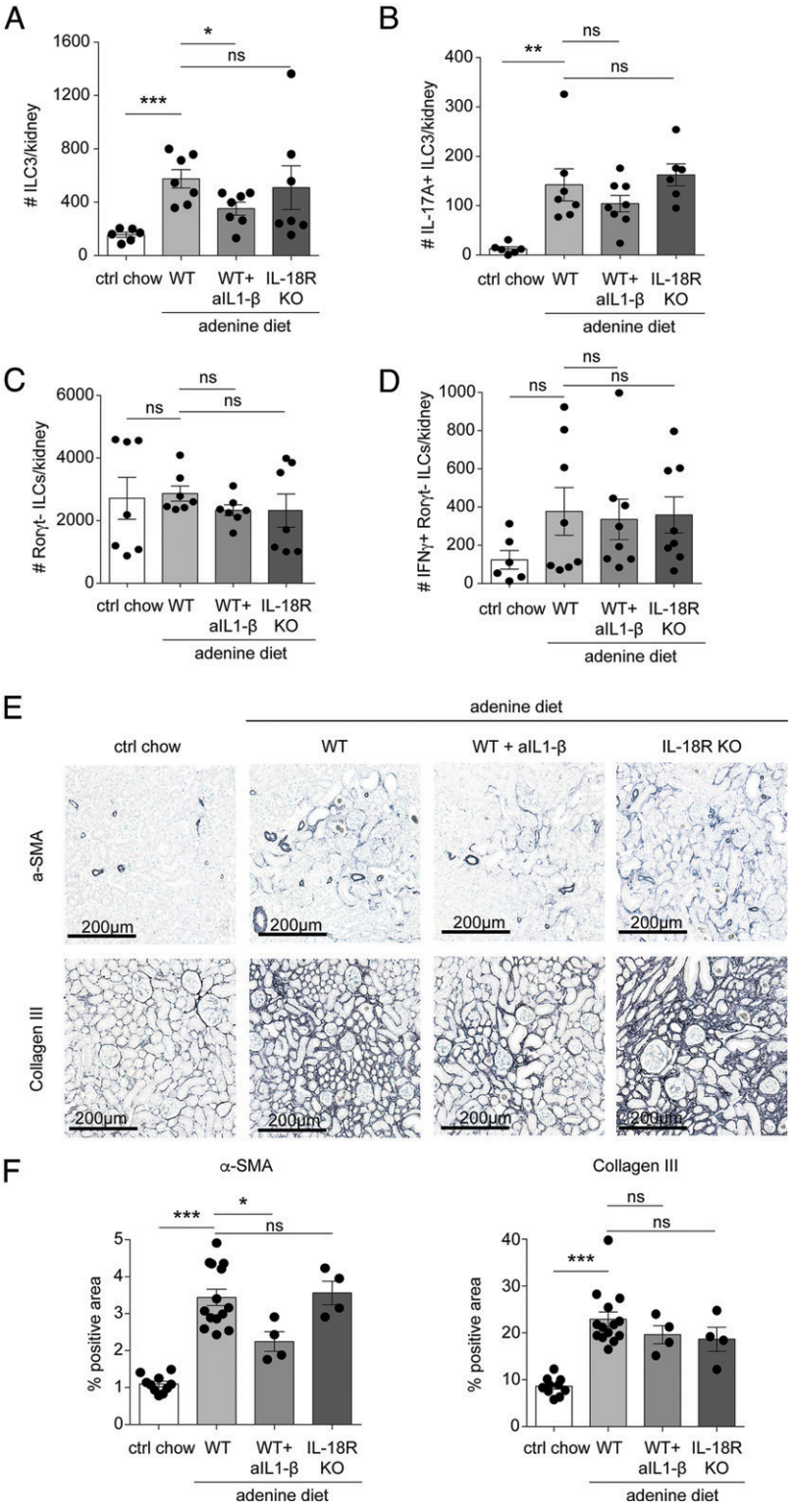


**FIGURE 3.** IL-1β, but not IL-18, expands intrarenal ILC3 and promotes crystal-induced kidney fibrosis. (**A**–**D**) Absolute numbers of renal ILC3s (A), IL-17-A$^+$ ILC3s (B), Rorγt$^-$ ILCs (C), and IFN-γ$^+$Rorγt$^-$ ILCs of WT mice (D) fed with control (ctrl) chow and WT mice, WT mice treated with 45 μg/mouse of an IL-1β–neutralizing Ab (depletion performed on days 1, 4, 7, and 10), and IL-18R KO mice fed with adenine diet for 14 d. Statistics were calculated using a one-way ANOVA with Tukey posttest ($n$ = 6–8 mice/group), $^*p < 0.05$, $^{**}p < 0.01$, $^{***}p < 0.001$. Data were pooled from two independent experiments and displayed as mean ± SEM. (**E**) Representative histology of α-SMA and Collagen III staining of kidney sections from WT mice on ctrl chow, WT mice, and WT mice treated with anti–IL-1β Ab, as well as IL-18R KO mice fed with adenine-enriched diet for 14 d (scale bars, 200 μm). (**F**) Percentages of positively stained areas for α-SMA and Collagen III of groups depicted in (E). Statistics were calculated using a one-way ANOVA with Tukey posttest ($n$ = 4–14 mice/group), $^*p < 0.05$, $^{***}p < 0.001$. Data were pooled from two independent experiments and displayed as mean ± SEM.

other ILC subtypes expressing this marker during inflammasome-mediated nephritis.

*Type 3 immunity promotes inflammasome-mediated kidney fibrosis*

To link inflammasome-mediated nephritis with type 3 immunity, we isolated MNPs from nephritic kidneys and measured their production of typical cytokines. MNPs of nephritic mice produced more IL-6, TGF-β, and IL-23 (Fig. 4A–C), all of which have been associated with differentiation of Rorγt$^+$ cells (70, 72, 73). Moreover, whole kidney homogenates of adenine-fed mice contained the type 3 cytokine IL-17A, consistent with the earlier findings (Fig. 1), whereas IL-22 and GM-CSF were unchanged (Fig. 4D–F).

Various innate and adaptive lymphocytes can secrete IL-17A (74, 75) and express Rorγt. To identify the IL-17A–producing cell type(s), we examined by flow cytometry three lymphocyte populations known to produce this cytokine: (1) αβ T cells (Thy1.2$^+$Rorγt$^+$lineage$^+$γδ TCR$^-$, including both Th17 cells and IL-17–producing CTLs), (2) γδ T cells (Thy1.2$^+$Rorγt$^+$lineage$^+$γδ TCR$^+$ population), and (3) ILC3s (Thy1.2$^+$Rorγt$^+$lineage$^-$γδ TCR$^-$ population) (Supplemental Fig. 6A). Rorγt$^+$IL-17$^+$ cells increased in

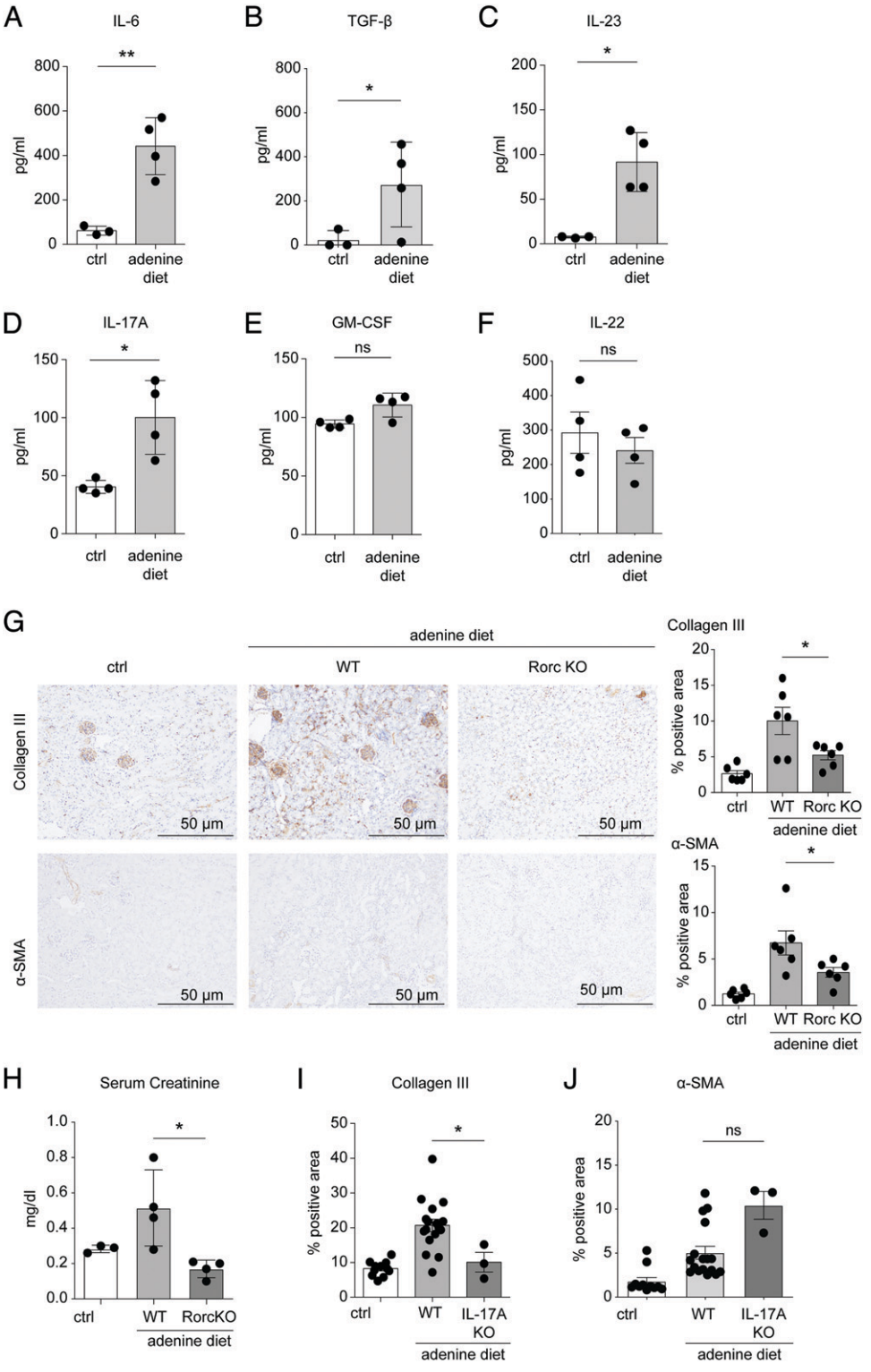


**FIGURE 4.** Type 3 immune cells promote inflammasome-mediated kidney fibrosis. (**A**–**C**) Cytokine concentration of IL-6 (A), TGF-β (B), and IL-23 (C) in supernatants of $CD11c^+$ renal MNPs from mice on control (ctrl chow) or adenine-enriched diet for 21 d, after culture for 24 h, determined by Luminex. Statistics were calculated using an unpaired Mann–Whitney *U* test ($n$ = 3–4 mice/group), $*p < 0.05$, $**p < 0.01$. One representative of two independent experiments was shown and depicted as mean ± SD. (**D**–**F**) Cytokine concentrations of IL-17A (D), GM-CSF (E), and IL-22 (F) in kidney homogenates of WT mice on ctrl or adenine-enriched diet for 21 d, measured by Luminex. Statistics were calculated using an unpaired Mann–Whitney *U* test ($n$ = 4 mice/group), $*p < 0.05$. One representative of two independent experiments was shown and depicted as mean ± SD. (**G**) Kidney sections stained for α-SMA and Collagen III from WT mice on ctrl chow, and from WT and Rorc KO mice fed with an adenine-enriched diet for 21 d. Calculation of the percentage of α-SMA–positive (**H**) or Collagen III–positive (**I**) areas. Statistics were calculated using a one-way ANOVA with Tukey posttest ($n$ = 6 mice/group), $*p < 0.05$. Data were pooled from two independent experiments and displayed as mean ± SEM. (H) Creatinine in the serum of indicated mice fed with ctrl or adenine-enriched diet. Statistics were calculated using a one-way ANOVA with Tukey posttest ($n$ = 3–4 mice/group), $*p < 0.05$. One representative of two independent experiments was shown and depicted as mean ± SD. (I and **J**) Quantification of Collagen III–positive (I) and α-SMA–positive (J) areas in kidney sections of WT and IL-17A KO mice fed with adenine-enriched diet for 14 d. Statistics were calculated using a one-way ANOVA with Tukey posttest ($n$ = 3–14 mice/group), $*p < 0.05$. Data were pooled from two independent experiments and displayed as mean ± SEM.

all three subsets in the kidneys of diseased mice (Supplemental Fig. 6B–D). When we measured IL-22 on protein and mRNA levels, no elevation was detected (Supplemental Fig. 7A, 7B). Furthermore, disease was not ameliorated in IL-22 KO mice, nor were renal ILC3s altered in comparison with WT mice (Supplemental Fig. 7C, 7D). Together with the data in Rag2KO mice treated with anti-Thy1.2 (Fig. 2), this indicated that $IL\text{-}17^+$ ILCs played a profibrotic role in our model.

To formally demonstrate a role of type 3 immunity, we fed Rorc KO mice that lack Rorγt the adenine-enriched diet. These animals developed less severe kidney fibrosis compared with WT mice, as evident by significantly lower α-SMA and Collagen III deposition in immunohistochemistry (Fig. 4G). Furthermore, Rorc KO mice showed significantly diminished creatinine serum (Fig. 4H). This confirmed that type 3 immune cells such as ILC3 were involved in inflammasome-mediated nephritis.

To test for a role of type 1 immunity, we fed the adenine-enriched diet to mice deficient for IFN-γ (IFN-γ KO). These mice showed similar deposition of α-SMA and Collagen III and similar serum creatinine as did WT mice (Supplemental

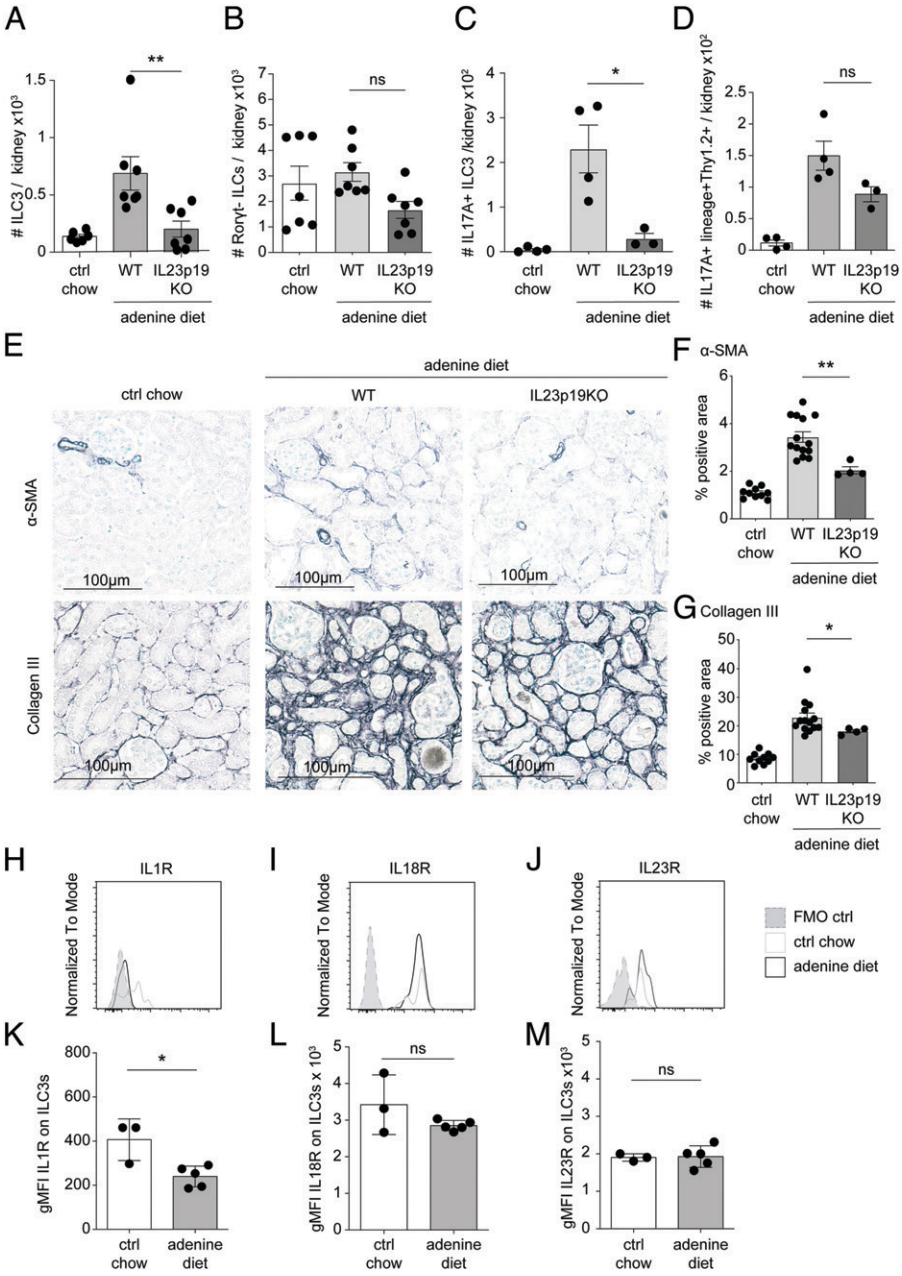


**FIGURE 5.** IL-23 maintains ILC3 and promotes crystal-induced kidney fibrosis. (**A** and **B**) Absolute cell numbers of renal ILC3 (A) and Rorγt$^-$ ILCs (B). Statistics were calculated using a one-way ANOVA with Tukey posttest ($n = 7$ mice/group), $^{**}p < 0.01$. Data were pooled from two independent experiments and displayed as mean ± SEM. (**C** and **D**) Number of either IL-17A$^+$ ILC3s (C) or of lineage$^+$ Thy1.2$^+$ cells (D) in healthy WT (control [ctrl] chow) and in IL-23p19 KO mice after 14 d of adenine diet. Statistics were calculated using a one-way ANOVA with Tukey posttest ($n$ = 3–4 mice/group), $^*p < 0.05$. One representative of two independent experiments was shown and depicted as mean ± SEM. (**E**) Representative α-SMA and Collagen III stainings of kidney sections from WT mice on normal chow (ctrl chow) and WT, as well as IL-23p19 KO mice on adenine-enriched diet for 14 d (scale bars, 100 μm). (**F** and **G**) Quantification of histological areas stained for α-SMA (F) and Collagen III (G) from mice depicted in (E). Statistics were calculated using a one-way ANOVA with Tukey posttest ($n$ = 4–14 mice/group), $^{**}p < 0.01$. Data were pooled from two independent experiments and displayed as mean ± SEM. (**H**–**J**) Representative histograms illustrating the expression of IL-1R, IL-23R, and IL-18R on ILC3 in the kidney of mice from ctrl diet (ctrl chow) or adenine diet assessed by flow cytometry. Fluorescence minus one ctrl (FMO) serves as ctrl (gray). (**K**–**M**) Geometric MFI (gMFI) of the molecular expression of IL-1R, IL-18R, and IL-23R on ILC3s. Statistics were calculated using an unpaired Mann–Whitney $U$ test ($n$ = 3–5 mice/group), $^*p < 0.05$. One representative of two independent experiments was shown and depicted as mean ± SD.

Fig. 8A–C), confirming that type 1 immunity was dispensable in our model.

*IL-23 maintains ILC3 during inflammasome-mediated nephritis and promotes fibrosis*

To determine which type 3 cytokines were important, we fed the adenine-enriched diet to mice deficient for IL-17A. We found reduced deposition of Collagen III, but no significant changes of α-SMA compared with WT mice (Fig. 4I, 4J), indicating partial protection from fibrosis. This may be explained by other type 3 effector cytokines that IL-17A–deficient mice still might be able to use. We therefore focused on IL-23, known to promote IL-17 production of ILC3, but not of other ILCs (32, 70, 72, 73). The kidneys of IL-23p19–deficient mice under the adenine diet contained 70% less ILC3 than WT mice (Fig. 5A), whereas Rorγt$^-$ ILC1 and ILC2 numbers were unchanged (Fig. 5B). Likewise, the IL-17A–producing ILC3 subset was reduced by even 85% (Fig. 5C), and other IL-17A–producing cells, determined as IL-17A$^+$lineage$^+$Thy1.2$^+$ cells, were not significantly reduced when IL-23 was lacking (Fig. 5D), arguing against major IL-23 effects on other type 3 immune cells, such as Th17 cells and γδ T cells in our model. Importantly, kidneys of IL-23p19–deficient mice showed significantly less staining for both α-SMA and Collagen III (Fig. 5E–G). These findings supported a pathogenic role of IL-23 in inflammasome-mediated nephritis.

To understand why IL-23 was more important for renal fibrosis than IL-1β in our model (Figs. 3, 5), we examined on renal ILC3 the expression of their receptors and of the IL-18R as a control. The receptors for IL-23 and IL-18 were expressed throughout the disease, whereas IL-1R was not detectable any longer on ILC3 after 14 d of adenine-enriched diet (Fig. 5H–M), implying that these cells had lost the ability to respond to IL-1β after activation. By contrast, they retained the capability to respond to IL-23, implying that this cytokine could affect ILC3 longer than IL-1β, possibly explaining the different effects.

*ILC3s colocalize with renal MNPs during sterile nephritis*

We next wished to visualize ILC3 in the nephritic kidney. To this end, we fed Rorc-reporter mice with the adenine-enriched diet and

analyzed kidney sections by multiepitope-ligand cartography. Automatized image analysis revealed Rorγt$^+$ cells that were lineage$^-$ (B220$^-$, Gr1$^-$, FcεR1a$^-$, CD11b$^-$, CD3$^-$) (Fig. 6A, white circles), classifying ILC3s. Notably, a certain proportion of these Rorγt$^+$ ILC3s were located in the vicinity of CD11b$^+$F4/80$^+$ MNPs during inflammasome-mediated nephritis. Computational image analysis showed that 8 of 10 ILC3s colocalized with MNPs in the section (80%) (Fig. 6B), whereas only 20 of 113 (17.7%) CD3$^+$ T cells, more precisely, 2 of 3 Th17 cells (66.7%), colocalized with MNPs (Fig. 6C), 4 of 10 ILC3s colocalized with CD3$^+$ T cells (Fig. 7D), and 3 of 15 (20%) Rorγt$^-$ ILC1s and ILC2s colocalized with MNPs (Supplemental Fig. 9). These findings suggested cross-talk between ILC3s and MNPs in inflammasome-mediated nephritis.

### *ILC3s cause renal MNPs to stimulate TGF-β production by fibroblasts in vitro*

Given that no tools exist to selectively remove ILC3 in vivo, we decided to directly demonstrate the profibrotic activity of ILC3 using a coculture system. Because ILC3s were very rare in the kidney, we instead purified renal CD11c$^+$F4/80$^+$ MNPs from mice under an adenine-enriched diet, which should have been influenced by ILC3, cocultured them with primary fibroblasts isolated from syngeneic mice, and measured their ability to stimulate collagen I release into the supernatant after 72 h (Fig. 7A). Indeed, renal MNPs from WT mice under an adenine-enriched diet stimulated fibroblasts to produce collagen I (Fig. 7B). Such production was seen also after adding the profibrotic cytokine TGF-β, which is produced by renal MNPs (76) (Fig. 7B), and it was reduced when a TGF-β–blocking Ab was added, but not when IL-1β was inhibited (Fig. 7B), arguing for TGF-β as a mediator of phagocyte-induced fibrosis. Importantly, neither phagocytes from RAG KO mice depleted with anti-Thy1.2 Ab from ILCs nor phagocytes from Rorc KO mice stimulated collagen production (Fig. 7C), consistent with the roles of ILCs and a type 3 immune response demonstrated in our in vivo studies (Figs. 2, 4). Furthermore, renal MNPs from mice lacking a functional IL-1β and IL-23 axis were unable to drive collagen production as much as phagocytes from WT mice (Fig. 7D), consistent with the fibrogenic role of these cytokines in vivo (Figs. 3, 5).

Finally, we aimed to directly demonstrate that ILC3s can render renal MNPs profibrogenic. To this end, we isolated ILCs precursors from mouse kidneys and differentiated them into ILC3s. Rorγt expression of the generated ILC3s was confirmed by flow cytometry (Supplemental Fig. 10). Such ILC3s were then cocultured with primary renal MNPs, followed by addition of fibroblasts as in the earlier experiments (Fig. 7E). After 72 h, ILC3-exposed renal MNPs stimulated collagen production by fibroblasts more than renal MNPs did, which were not exposed to ILC3s or to Rorγt$^-$ ILCs (Fig. 7F), confirming the ability of ILC3s to promote the profibrotic properties of renal MNPs. In summary, these findings support the scenario that inflammasome-stimulated ILC3s interacted via IL-1β or IL-23 with renal MNPs, which then used TGF-β to promote renal fibrosis.

## Discussion

Fibrosis is a common consequence of inflammasome activation and chronic inflammation in several tissues (77), including the kidney (6, 9, 56, 78, 79). In this article, we propose a (to our knowledge) novel pathway how inflammasome activation can promote kidney fibrosis via ILC3s that respond to the inflammasome-derived cytokine, IL-1β, and to the type 3 immunity cytokine, IL-23, which emerged as an amplifier of NLRP3 inflammasome activation and resultant kidney fibrosis. These findings were unexpected because fibrosis is usually associated with type 2 immunity. Consistently, ILC2 promoted tissue repair in Adriamycin-induced murine glomerulosclerosis (43, 52). We found no upregulation of type 2 cytokines in our model, which argued against a role of ILC2 but did not formally exclude an additional role of these cells. ILC3s have very recently been implicated in lupus nephritis (54) and unilateral ureteral obstruction (55), but a role in inflammasome-dependent kidney inflammation has not been described yet.

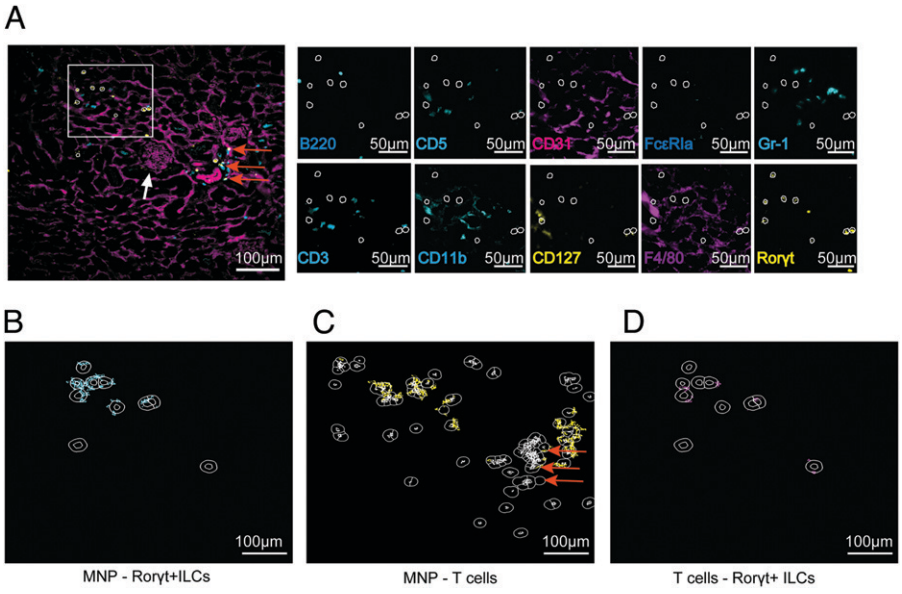


**FIGURE 6.** Visualization of intrarenal ILC3s and colocalization with renal MNPs. (**A**–**D**) Multiplexed histological images of a representative kidney section, where computationally identified ILC3s, defined as Rorγt$^+$lineage$^-$ (B220$^-$, CD5$^-$, Gr1$^-$, FcεR1a$^-$, CD11b$^-$, CD3$^-$) cells, were shown as white circles. The white arrow marks a glomerulus. The immunofluorescence overlay depicts CD3 (cyan), CD31 (magenta), and Rorγt (yellow), and a region of interest (ROI) is indicated as a white square. Single staining for all relevant markers included in the multiplexed histology are shown for the ROI (ILC inclusion markers in yellow, exclusion markers in cyan, and other markers in magenta). Neighborhood analysis of the ILC3s detected as described in (A) with renal MNPs (B), or T cells with renal MNPs (CD45$^+$F4/80$^+$CD11b$^+$ cells) (C) and ILC3s with T cells (CD45$^+$CD3$^+$ cells) (D) found within a 10-μm radius (considered as neighborhood and shown as white circles). Neighborhood cells around each ILC3 are shown in cyan (B) and magenta (D). Orange arrows in (A) and (C) mark CD3$^+$Rorγt$^+$ Th17 cells.

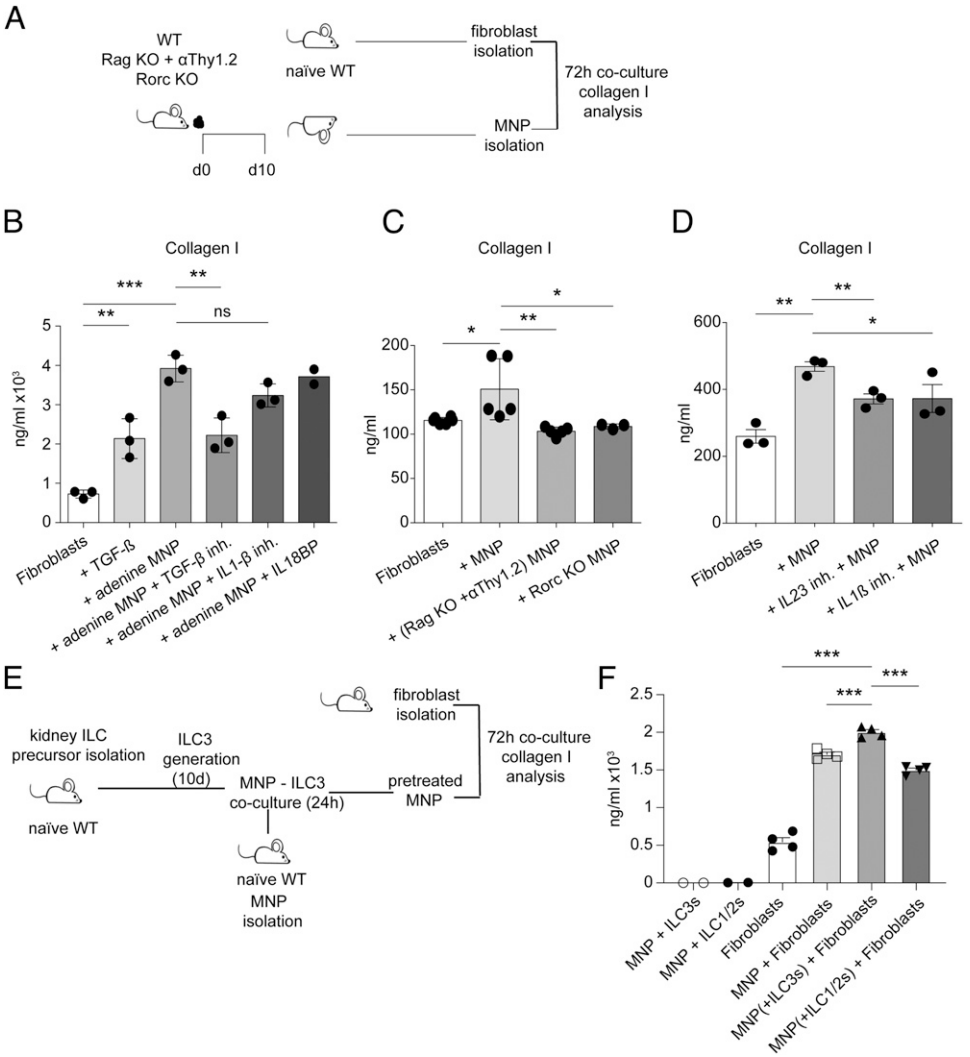


**FIGURE 7.** ILC3s modulate renal MNPs to stimulate Collagen I release by fibroblasts. (**A**) Experimental design of fibroblast-renal MNP coculture used in experiments shown in (**B**)–(**D**). (B) Collagen I production released during fibroblasts-renal MNPs 72-h coculture in the presence of TGF-β inhibitor, IL-1β inhibitor, or IL-18 binding protein (IL-18BP). Or fibroblasts stimulated with TGF-β as control. (C) Collagen I production measured by ELISA during 72-h fibroblasts-renal MNP cultures isolated from indicated genetically modified mouse lines on adenine-enriched diet. (D) Collagen I production released during 72-h fibroblasts-renal MNP coculture in the presence of an IL-23 (IL-23 inh.) or IL-1β inhibitor (IL-1β inh.). (**E**) In vitro experimental design of ILC3-fibroblast-renal MNP cocultures used in (**F**). (F) Collagen I production measured by ELISA during 72-h fibroblast-renal MNP coculture. MNPs were preincubated with in vitro–differentiated ILC3 or ILC1/2 for 72 h. Statistics were calculated using a one-way ANOVA with Tukey posttest ($n = 2–5$ mice/group), $^{**}p < 0.01$. One representative of two independent experiments was shown and depicted as mean ± SEM.

The type 3 signature cytokine IL-17 has been shown to promote fibrosis in other contexts, like liver fibrosis (49) or unilateral ureteral obstruction (40, 55). However, it played only a partial profibrotic role in our model, which was reminiscent of the situation in multiple sclerosis, where Th17 cells are important for disease, but not because of their production of IL-17 (80), but of GM-CSF (81). However, in our model, GM-CSF was not increased. Instead, the type 3 immunity maintenance cytokine IL-23 played a major profibrotic role in our system, as did the signature inflammasome cytokine IL-1β, which expanded ILC3. This finding was consistent with previous work showing that this cytokine induced expansion of pulmonary ILC3 in a mouse model of obesity-associated airway hyperactivity (67). ILC3s express a broad range of cytokine receptors, including IL-1R, IL-18R, and Il-23R (67, 82), explaining their response to inflammasome products (83, 84). However, the IL-1R was downregulated during the course of disease, perhaps as a result of receptor endocytosis upon ligand binding (85–87), so that it could no longer stimulate ILC3s. By contrast, sustained IL-23R expression may explain the greater protection seen in mice lacking IL-23 than IL-1β. Another explanation may be an effect of IL-23, but not IL-1β, on Th17 and/or γδ T cells, although we did not detect significant alterations in their numbers. Adaptive type 3 immune cells also played a role in our model and depend on IL-23 (32, 59). Future studies are warranted to address their role in inflammasome-mediated fibrosis.

Sustained expression was also noted for the receptor of IL-18, the other main inflammasome-derived cytokine. However, genetic removal of this receptor failed to affect renal ILC3 numbers and cytokine production. In this respect, ILC3s seem to differ from NK cells and ILC1, which did proliferate in other models in response to IL-18 (88, 89). Consistent with the role of ILC3, inflammasome-mediated fibrosis did not depend on IL-18. This contrasts with the situation in acute crystal-induced kidney injury, where IL-18 did play a role (8). IL-18 affected NKp46 expression on ILCs, as it did in NK cells, but this did not noticeably impact fibrosis development in our model. We did not use fate-mapping mouse models to formally prove the conversion of NKp46$^{-}$ ILCs in NKp46$^{+}$ ILCs or to determine the relationship between ILC3 and NK cells (90, 91), but focused on changes of NKp46$^{+}$ ILC3s in the presence or absence of IL-18 during inflammasome-mediated inflammation. To mechanistically unravel the role of the NKp46$^{+}$ ILC3 subpopulation, tools need to be developed to generate mice exclusively lacking NKp46 in ILC3s.

The cross-talk between ILC3s and renal MNPs was supported by the analysis of these cells in their tissue context by multiplexed histology, an imaging technique coupled to a customized analysis pipeline that allowed us to computationally analyze and quantify single cells within tissues, while retaining their spatial information. This analysis showed colocalization between ILC3s and renal MNPs in inflamed kidneys. The molecular pathways identified during our

in vivo experiments were further corroborated by in vitro studies, where we queried the ability of renal MNPs isolated from mice with adenine-induced nephritis to elicit collagen production by cocultured fibroblasts. Such production was lower when the MNPs were obtained from nephritic mice lacking ILC, Rorc, IL-1β or IL-23, providing further experimental support for the pathomechanism we identified in this study. This mechanism is consistent with the recent proposal that ILC3-derived cytokines may support tissue homeostasis by inducing immunosuppressive and/or repair functions of MNPs (47, 92) and with the recent identification of a type 3 immunity-related profibrotic macrophage subset in the liver and lung (93). An exaggerated repair function triggered by NLRP3 inflammasome activation may cause ILC3s to promote renal MNP-driven fibrosis. Our in vitro studies suggested that fibroblasts are instructed by TGF-β, a long-known critical mediator of kidney fibrosis (76). This finding differs from a recent study proposing that ILC3s use IL-17A to stimulate fibroblasts (55), which was not the case in our model. Further studies are needed to clarify how ILC3s cause MNPs to produce TGF-β.

In conclusion, ILC3, IL-23, and IL-1β are mediators in inflammasome-mediated fibrosis in the kidney and perhaps also in other organs and might represent therapeutic targets.

## Acknowledgments

We acknowledge support by the Flow Cytometry Core Facility and the central animal facilities of the Medical Faculty of Bonn University. We especially thank Andreas Diefenbach (Charité) for help with in vitro expansion of ILC3. The visual abstract was created using BioRender.com.

## Disclosures

The authors have no financial conflicts of interest.

## References

1. Lamkanfi, M., and V. M. Dixit. 2012. Inflammasomes and their roles in health and disease. *Annu. Rev. Cell. Dev. Biol.* 28: 137–161.
2. Rathinam, V. A., and K. A. Fitzgerald. 2016. Inflammasome complexes: emerging mechanisms and effector functions. *Cell* 165: 792–800.
3. Zhang, W. J., S. J. Chen, S. C. Zhou, S. Z. Wu, and H. Wang. 2021. Inflammasomes and fibrosis. *Front. Immunol.* 12: 643149.
4. Moeller, M. J., R. Kramann, T. Lammers, B. Hoppe, E. Latz, I. Ludwig-Portugall, P. Boor, J. Floege, C. Kurts, R. Weiskirchen, and T. Ostendorf. 2021. New aspects of kidney fibrosis—from mechanisms of injury to modulation of disease. *Front. Med. (Lausanne)* 8: 814497.
5. Labzin, L. I., M. T. Heneka, and E. Latz. 2018. Innate immunity and neurodegeneration. *Annu. Rev. Med.* 69: 437–449.
6. Mulay, S. R., and H. J. Anders. 2017. Crystal nephropathies: mechanisms of crystal-induced kidney injury. *Nat. Rev. Nephrol.* 13: 226–240.
7. Kurts, C., U. Panzer, H. J. Anders, and A. J. Rees. 2013. The immune system and kidney disease: basic concepts and clinical implications. *Nat. Rev. Immunol.* 13: 738–753.
8. Mulay, S. R., O. P. Kulkarni, K. V. Rupanagudi, A. Migliorini, M. N. Darisipudi, A. VILaysane, D. Muruve, Y. Shi, F. Munro, H. Liapis, and H. J. Anders. 2013. Calcium oxalate crystals induce renal inflammation by NLRP3-mediated IL-1β secretion. *J. Clin. Invest.* 123: 236–246.
9. Knauf, F., J. R. Asplin, I. Granja, I. M. Schmidt, G. W. Moeckel, R. J. David, R. A. Flavell, and P. S. Aronson. 2013. NALP3-mediated inflammation is a principal cause of progressive renal failure in oxalate nephropathy. *Kidney Int.* 84: 895–901.
10. Komada, T., and D. A. Muruve. 2019. The role of inflammasomes in kidney disease. *Nat. Rev. Nephrol.* 15: 501–520.
11. Yin, J., Q. Mei, M. Prinz, Z. Abdullah, U. Panzer, J. Li, S. von Vietinghoff, and C. Kurts. 2023. Fate mapping reveals compartment-specific clonal expansion of mononuclear phagocytes during kidney disease. *Kidney. Int.* 104: 605–610.
12. Nikolic-Paterson, D. J., and R. C. Atkins. 2001. The role of macrophages in glomerulonephritis. *Nephrol. Dial. Transplant* 16(Suppl 5): 3–7.
13. Tittel, A. P., C. Heuser, C. Ohliger, P. A. Knolle, D. R. Engel, and C. Kurts. 2011. Kidney dendritic cells induce innate immunity against bacterial pyelonephritis. *J. Am. Soc. Nephrol.* 22: 1435–1441.
14. Lukacs-Kornek, V., S. Burgdorf, L. Diehl, S. Specht, M. Kornek, and C. Kurts. 2008. The kidney-renal lymph node-system contributes to cross-tolerance against innocuous circulating antigen. *J. Immunol.* 180: 706–715.
15. Kurts, C., F. Ginhoux, and U. Panzer. 2020. Kidney dendritic cells: fundamental biology and functional roles in health and disease. *Nat. Rev. Nephrol.* 16: 391–407.
16. Klinkhammer, B. M., S. Buchtler, S. Djudjaj, N. Bouteldja, R. Palsson, V. O. Edvardsson, M. Thorsteinsdottir, J. Floege, M. Mack, and P. Boor. 2022. Current kidney function parameters overestimate kidney tissue repair in reversible experimental kidney disease. *Kidney Int.* 102: 307–320.
17. Coll, R. C., A. A. Robertson, J. J. Chae, S. C. Higgins, R. Muñoz-Planillo, M. C. Inserra, I. Vetter, L. S. Dungan, B. G. Monks, A. Stutz, et al. 2015. A small-molecule inhibitor of the NLRP3 inflammasome for the treatment of inflammatory diseases. *Nat. Med.* 21: 248–255.
18. Ludwig-Portugall, I., E. Bartok, E. Dhana, B. D. Evers, M. J. Primiano, J. P. Hall, B. S. Franklin, P. A. Knolle, V. Hornung, G. Hartmann, et al. 2016. An NLRP3-specific inflammasome inhibitor attenuates crystal-induced kidney fibrosis in mice. *Kidney Int.* 90: 525–539.
19. Agoro, R., J. Piotet-Morin, J. Palomo, C. Michaudel, S. Vigne, I. Maillet, P. Chenuet, N. Guillou, J. L. Bérichel, M. Kisielow, et al. 2016. IL-1R1-MyD88 axis elicits papain-induced lung inflammation. *Eur. J. Immunol.* 46: 2531–2541.
20. Soare, A., S. Weber, L. Maul, S. Rauber, A. M. Gheorghiu, M. Luber, I. Houssni, A. Kleyer, G. von Pickardt, M. Gado, et al. 2018. Cutting edge: homeostasis of innate lymphoid cells is imbalanced in psoriatic arthritis. *J. Immunol.* 200: 1249–1254.
21. Rauber, S., M. Luber, S. Weber, L. Maul, A. Soare, T. Wohlfahrt, N. Y. Lin, K. Dietel, A. Bozec, M. Herrmann, et al. 2017. Resolution of inflammation by interleukin-9-producing type 2 innate lymphoid cells. *Nat. Med.* 23: 938–944.
22. Omata, Y., M. Frech, T. Primbs, S. Lucas, D. Andreev, C. Scholtysek, K. Sarter, M. Kindermann, N. Yeremenko, D. L. Baeten, et al. 2018. Group 2 innate lymphoid cells attenuate inflammatory arthritis and protect from bone destruction in mice. *Cell. Rep.* 24: 169–180.
23. Spits, H., D. Artis, M. Colonna, A. Diefenbach, J. P. Di Santo, G. Eberl, S. Koyasu, R. M. Locksley, A. N. McKenzie, R. E. Mebius, et al. 2013. Innate lymphoid cells—a proposal for uniform nomenclature. *Nat. Rev. Immunol.* 13: 145–149.
24. Bedoui, S., T. Gebhardt, G. Gasteiger, and W. Kastenmüller. 2016. Parallels and differences between innate and adaptive lymphocytes. *Nat. Immunol.* 17: 490–494.
25. Cortez, V. S., and M. Colonna. 2016. Diversity and function of group 1 innate lymphoid cells. *Immunol. Lett.* 179: 19–24.
26. Eberl, G., J. P. Di Santo, and E. Vivier. 2015. The brave new world of innate lymphoid cells. *Nat. Immunol.* 16: 1–5.
27. Vivier, E., D. Artis, M. Colonna, A. Diefenbach, J. P. Di Santo, G. Eberl, S. Koyasu, R. M. Locksley, A. N. J. McKenzie, R. E. Mebius, et al. 2018. Innate lymphoid cells: 10 years on. *Cell* 174: 1054–1066.
28. Fuchs, A., W. Vermi, J. S. Lee, S. Lonardi, S. Gilfillan, R. D. Newberry, M. Cella, and M. Colonna. 2013. Intraepithelial type 1 innate lymphoid cells are a unique subset of IL-12- and IL-15-responsive IFN-γ-producing cells. *Immunity* 38: 769–781.
29. Klose, C. S. N., M. Flach, L. Möhle, L. Rogell, T. Hoyler, K. Ebert, C. Fabiunke, D. Pfeifer, V. Sexl, D. Fonseca-Pereira, et al. 2014. Differentiation of type 1 ILCs from a common progenitor to all helper-like innate lymphoid cell lineages. *Cell* 157: 340–356.
30. Mjösberg, J., J. Bernink, C. Peters, and H. Spits. 2012. Transcriptional control of innate lymphoid cells. *Eur. J. Immunol.* 42: 1916–1923.
31. Atreya, I., M. Kindermann, and S. Wirtz. 2019. Innate lymphoid cells in intestinal cancer development. *Semin. Immunol.* 41: 101267.
32. Bernink, J. H., L. Krabbendam, K. Germar, E. de Jong, K. Gronke, M. Kofoed-Nielsen, J. M. Munneke, M. D. Hazenberg, J. Villaudy, C. J. Buskens, et al. 2015. Interleukin-12 and -23 control plasticity of CD127(+) group 1 and group 3 innate lymphoid cells in the intestinal lamina propria. *Immunity* 43: 146–160.
33. Killig, M., T. Glatzer, and C. Romagnani. 2014. Recognition strategies of group 3 innate lymphoid cells. *Front. Immunol.* 5: 142.
34. Cording, S., J. Medvedovic, M. Cherrier, and G. Eberl. 2014. Development and regulation of RORγt(+) innate lymphoid cells. *FEBS. Lett.* 588: 4176–4181.
35. Aparicio-Domingo, P., and T. Cupedo. 2011. Rorγt+ innate lymphoid cells in intestinal homeostasis and immunity. *J. Innate Immun.* 3: 577–584.
36. Sawa, S., M. Lochner, N. Satoh-Takayama, S. Dulauroy, M. Bérard, M. Kleinschek, D. Cua, J. P. Di Santo, and G. Eberl. 2011. RORγt+ innate lymphoid cells regulate intestinal homeostasis by integrating negative signals from the symbiotic microbiota. *Nat. Immunol.* 12: 320–326.
37. Coulter, F., A. Parrish, D. Manning, B. Kampmann, J. Mendy, M. Garand, D. M. Lewinsohn, E. M. Riley, and J. S. Sutherland. 2017. IL-17 production from T helper 17, mucosal-associated invariant T, and γδ cells in tuberculosis infection and disease. *Front. Immunol.* 8: 1252.
38. Cua, D. J., and C. M. Tato. 2010. Innate IL-17-producing cells: the sentinels of the immune system. *Nat. Rev. Immunol.* 10: 479–489.
39. Krebs, C. F., J. E. Turner, H. J. Paust, S. Kapffer, T. Koyro, S. Krohn, F. Ufer, M. A. Friese, R. A. Flavell, B. Stockinger, et al. 2016. Plasticity of Th17 cells in autoimmune kidney diseases. *J. Immunol.* 197: 449–457.
40. Peng, X., Z. Xiao, J. Zhang, Y. Li, Y. Dong, and J. Du. 2015. IL-17A produced by both gammadelta T and Th17 cells promotes renal fibrosis via RANTES-mediated leukocyte infiltration after renal obstruction. *J. Pathol.* 235: 79–89.
41. Mi, S., Z. Li, H. Z. Yang, H. Liu, J. P. Wang, Y. G. Ma, X. X. Wang, H. Z. Liu, W. Sun, and Z. W. Hu. 2011. Blocking IL-17A promotes the resolution of pulmonary inflammation and fibrosis via TGF-beta1-dependent and -independent mechanisms. *J. Immunol.* 187: 3003–3014.
42. Artis, D., and H. Spits. 2015. The biology of innate lymphoid cells. *Nature* 517: 293–301.
43. Riedel, J. H., M. Becker, K. Kopp, M. Düster, S. R. Brix, C. Meyer-Schwesinger, L. A. Kluth, A. C. Gnirck, M. Attar, S. Krohn, et al. 2017. IL-33-mediated expansion of type 2 innate lymphoid cells protects from progressive glomerulosclerosis. *J. Am. Soc. Nephrol.* 28: 2068–2080.

44. Hoyler, T., C. A. Connor, E. A. Kiss, and A. Diefenbach. 2013. T-bet and Gata3 in controlling type 1 and type 2 immunity mediated by innate lymphoid cells. *Curr. Opin. Immunol.* 25: 139–147.
45. Gasteiger, G., X. Fan, S. Dikiy, S. Y. Lee, and A. Y. Rudensky. 2015. Tissue residency of innate lymphoid cells in lymphoid and nonlymphoid organs. *Science* 350: 981–985.
46. Klose, C. S. N., and D. Artis. 2020. Innate lymphoid cells control signaling circuits to regulate tissue-specific immunity. *Cell. Res.* 30: 475–491.
47. Mortha, A., and K. Burrows. 2018. Cytokine networks between innate lymphoid cells and myeloid cells. *Front. Immunol.* 9: 191.
48. Ardain, A., J. Z. Porterfield, H. N. Kløverpris, and A. Leslie. 2019. Type 3 ILCs in lung disease. *Front. Immunol.* 10: 92.
49. Tait Wojno, E. D., and D. Artis. 2012. Innate lymphoid cells: balancing immunity, inflammation, and tissue repair in the intestine. *Cell Host Microbe* 12: 445–457.
50. Wang, R., Y. Wang, D. C. H. Harris, and Q. Cao. 2021. Innate lymphoid cells in kidney diseases. *Kidney Int.* 99: 1077–1087.
51. Becker, M., A. C. Gnirck, and J. E. Turner. 2020. Innate lymphoid cells in renal inflammation. *Front. Immunol.* 11: 72.
52. Nagashima, R., and M. Iyoda. 2021. The roles of kidney-resident ILC2 in renal inflammation and fibrosis. *Front. Immunol.* 12: 688647.
53. Ryu, S., and H. Y. Kim. 2023. Bone marrow progenitors and IL-2 signaling contribute to the strain differences of kidney innate lymphoid cells. *Immune Netw.* 23: e15.
54. Li, F., Z. Liang, H. Zhong, X. Hu, Z. Tang, C. Zhu, J. Shen, X. Han, R. Lin, R. Zheng, et al. 2023. Group 3 innate lymphoid cells exacerbate lupus nephritis by promoting B cell activation in kidney ectopic lymphoid structures. *Adv. Sci. (Weinh)*10: e2302804.
55. Liang, Z., Z. Tang, C. Zhu, F. Li, S. Chen, X. Han, R. Zheng, X. Hu, R. Lin, Q. Pei, et al. 2024. Intestinal CXCR6(+) ILC3s migrate to the kidney and exacerbate renal fibrosis via IL-23 receptor signaling enhanced by PD-1 expression. *Immunity.* 57: 1306–1323.e8.
56. Dhana, E., I. Ludwig-Portugall, and C. Kurts. 2018. Role of immune cells in crystal-induced kidney fibrosis. *Matrix Biol.* 68-69: 280–292.
57. Ivanov, I. I., B. S. McKenzie, L. Zhou, C. E. Tadokoro, A. Lepelley, J. J. Lafaille, D. J. Cua, and D. R. Littman. 2006. The orphan nuclear receptor RORgammat directs the differentiation program of proinflammatory IL-17+ T helper cells. *Cell* 126: 1121–1133.
58. Hoshino, K., H. Tsutsui, T. Kawai, K. Takeda, K. Nakanishi, Y. Takeda, and S. Akira. 1999. Cutting edge: generation of IL-18 receptor-deficient mice: evidence for IL-1 receptor-related protein as an essential IL-18 binding receptor. *J. Immunol.* 162: 5041–5044.
59. Turner, J. E., C. Krebs, A. P. Tittel, H. J. Paust, C. Meyer-Schwesinger, S. B. Bennstein, O. M. Steinmetz, I. Prinz, T. Magnus, T. Korn, et al. 2012. IL-17A production by renal γδ T cells promotes kidney injury in crescentic GN. *J. Am. Soc. Nephrol.* 23: 1486–1495.
60. Ahlfors, H., P. J. Morrison, J. H. Duarte, Y. Li, J. Biro, M. Tolaini, P. Di Meglio, A. J. PotoCNik, and B. Stockinger. 2014. IL-22 fate reporter reveals origin and control of IL-22 production in homeostasis and infection. *J. Immunol.* 193: 4602–4613.
61. Ghilardi, N., N. Kljavin, Q. Chen, S. Lucas, A. L. Gurney, and F. J. de Sauvage. 2004. Compromised humoral and delayed-type hypersensitivity responses in IL-23-deficient mice. *J. Immunol.*172: 2827–2833.
62. Hochheiser, K., D. R. Engel, L. Hammerich, F. Heymann, P. A. Knolle, U. Panzer, and C. Kurts. 2011. Kidney dendritic cells become pathogenic during crescentic glomerulonephritis with proteinuria. *J. Am. Soc. Nephrol.* 22: 306–316.
63. Sun, Q., M. Baues, B. M. Klinkhammer, J. Ehling, S. Djudjaj, N. I. Drude, C. Daniel, K. Amann, R. Kramann, H. Kim, et al. 2019. Elastin imaging enables noninvasive staging and treatment monitoring of kidney fibrosis. *Sci. Transl. Med.* 11: eaat4865.
64. Holzwarth, K., R. Köhler, L. Philipsen, K. Tokoyoda, V. Ladyhina, C. Wählby, R. A. NIEsner, and A. E. Hauser. 2018. Multiplexed fluorescence microscopy reveals heterogeneity among stromal cells in mouse bone marrow sections. *Cytometry A* 93: 876–888.
65. Krebs, C. F., T. Schmidt, J. H. Riedel, and U. Panzer. 2017. T helper type 17 cells in immune-mediated glomerular disease. *Nat. Rev. Nephrol.* 13: 647–659.
66. Tamura, M., R. Aizawa, M. Hori, and H. Ozaki. 2009. Progressive renal dysfunction and macrophage infiltration in interstitial fibrosis in an adenine-induced tubulo-interstitial nephritis mouse model. *Histochem. Cell. Biol.* 131: 483–490.
67. Kim, H. Y., H. J. Lee, Y. J. Chang, M. Pichavant, S. A. Shore, K. A. Fitzgerald, Y. Iwakura, E. Israel, K. Bolger, J. Faul, et al. 2014. Interleukin-17-producing innate lymphoid cells and the NLRP3 inflammasome facilitate obesity-associated airway hyperreactivity. *Nat. Med.* 20: 54–61.
68. Buonocore, S., P. P. Ahern, H. H. Uhlig, I. I. Ivanov, D. R. Littman, K. J. Maloy, and F. Powrie. 2010. Innate lymphoid cells drive interleukin-23-dependent innate intestinal pathology. *Nature* 464: 1371–1375.
69. Powell, N., J. W. Lo, P. Biancheri, A. Vossenkamper, E. Pantazi, A. W. Walker, E. Stolarczyk, F. Ammoscato, R. Goldberg, P. Scott, et al. 2015. Interleukin 6 increases production of cytokines by colonic innate lymphoid cells in mice and patients with chronic intestinal inflammation. *Gastroenterology* 149: 456–467.e15.
70. Ikeda, S., S. Saijo, M. A. Murayama, K. Shimizu, A. Akitsu, and Y. Iwakura. 2014. Excess IL-1 signaling enhances the development of Th17 cells by downregulating TGF-β-induced Foxp3 expression. *J. Immunol.* 192: 1449–1458.
71. Kühnel, I., I. Vogler, J. Spreu, H. Bonig, C. Döring, and A. Steinle. 2024. The activating receptor NKp65 is selectively expressed by human ILC3 and demarcates ILC3 from mature NK cells. *Eur. J. Immunol.* 54: e2250318.
72. Zhou, L., I. I. Ivanov, R. Spolski, R. Min, K. Shenderov, T. Egawa, D. E. Levy, W. J. Leonard, and D. R. Littman. 2007. IL-6 programs T(H)-17 cell differentiation by promoting sequential engagement of the IL-21 and IL-23 pathways. *Nat. Immunol.* 8: 967–974.
73. Golebski, K., X. R. Ros, M. Nagasawa, S. van Tol, B. A. Heesters, H. Aglmous, C. M. A. Kradolfer, M. M. Shikhagaie, S. Seys, P. W. Hellings, et al. 2019. IL-1β, IL-23, and TGF-β drive plasticity of human ILC2s towards IL-17-producing ILCs in nasal inflammation. *Nat. Commun.* 10: 2162.
74. Rutz, S., C. Eidenschenk, J. R. Kiefer, and W. Ouyang. 2016. Post-translational regulation of RORγt-A therapeutic target for the modulation of interleukin-17-mediated responses in autoimmune diseases. *Cytokine Growth Factor Rev.* 30: 1–17.
75. Sun, Z., D. Unutmaz, Y. R. Zou, M. J. Sunshine, A. Pierani, S. Brenner-Morton, R. E. MebIUs, and D. R. Littman. 2000. Requirement for RORgamma in thymocyte survival and lymphoid organ development. *Science* 288: 2369–2373.
76. Gu, Y.-Y., X.-S. Liu, X.-R. Huang, X.-Q. Yu, and H.-Y. Lan. 2020. Diverse role of TGF-β in kidney disease. *Front. Cell. Dev. Biol.* 8: 123.
77. Latz, E. 2010. The inflammasomes: mechanisms of activation and function. *Curr. Opin. Immunol.* 22: 28–33.
78. Khan, S. R. 2004. Crystal-induced inflammation of the kidneys: results from human studies, animal models, and tissue-culture studies. *Clin. Exp. Nephrol.* 8: 75–88.
79. Mulay, S. R., A. Evan, and H. J. Anders. 2014. Molecular mechanisms of crystal-related kidney inflammation and injury. Implications for cholesterol embolism, crystalline nephropathies and kidney stone disease. *Nephrol. Dial. Transplant* 29: 507–514.
80. Haak, S., A. L. Croxford, K. Kreymborg, F. L. Heppner, S. Pouly, B. Becher, and A. Waisman. 2009. IL-17A and IL-17F do not contribute vitally to autoimmune neuro-inflammation in mice. *J. Clin. Invest.* 119: 61–69.
81. Becher, B., S. Tugues, and M. Greter. 2016. GM-CSF: from growth factor to central mediator of tissue inflammation. *Immunity* 45: 963–973.
82. Ohne, Y., J. S. Silver, L. Thompson-Snipes, M. A. Collet, J. P. Blanck, B. L. Cantarel, A. M. Copenhaver, A. A. Humbles, and Y.-J. Liu. 2016. IL-1 is a critical regulator of group 2 innate lymphoid cell function and plasticity. *Nat. Immunol.* 17: 646–655.
83. Robinette, M. L., A. Fuchs, V. S. Cortez, J. S. Lee, Y. Wang, S. K. Durum, S. Gilfillan, and M. Colonna; Immunological Genome Consortium. 2015. Transcriptional programs define molecular characteristics of innate lymphoid cell classes and subsets. *Nat. Immunol.* 16: 306–317.
84. Klose, C. S., and D. Artis. 2016. Innate lymphoid cells as regulators of immunity, inflammation and tissue homeostasis. *Nat. Immunol.* 17: 765–774.
85. Hansen, B., O. Dittrich-Breiholz, M. Kracht, and M. Windheim. 2013. Regulation of NF-κB-dependent gene expression by ligand-induced endocytosis of the interleukin-1 receptor. *Cell. Signal.* 25: 214–228.
86. Brissoni, B., L. Agostini, M. Kropf, F. Martinon, V. Swoboda, S. Lippens, H. Everett, N. Aebi, S. Janssens, E. Meylan, et al. 2006. Intracellular trafficking of interleukin-1 receptor I requires Tollip. *Curr. Biol.* 16: 2265–2270.
87. Dunne, A., and L. A. J. O'Neill. 2003. The interleukin-1 receptor/Toll-like receptor superfamily: signal transduction during inflammation and host defense. *Sci. STKE* 2003: re3.
88. French, A. R., E. B. Holroyd, L. Yang, S. Kim, and W. M. Yokoyama. 2006. IL-18 acts synergistically with IL-15 in stimulating natural killer cell proliferation. *Cytokine* 35: 229–234.
89. Li, W., H. Yamamoto, S. Kubo, and H. Okamura. 2009. Modulation of innate immunity by IL-18. *J. Reprod. Immunol.* 83: 101–105.
90. Vonarbourg, C., A. Mortha, V. L. Bui, P. P. Hernandez, E. A. Kiss, T. Hoyler, M. Flach, B. Bengsch, R. Thimme, C. Hölscher, et al. 2010. Regulated expression of nuclear receptor RORγt confers distinct functional fates to NK cell receptor-expressing RORγt(+) innate lymphocytes. *Immunity* 33: 736–751.
91. Verrier, T., N. Satoh-Takayama, N. Serafini, S. Marie, J. P. Di Santo, and C. A. J. Vosshenrich. 2016. Phenotypic and functional plasticity of murine intestinal NKp46+ group 3 innate lymphoid cells. *J. Immunol.* 196: 4731–4738.
92. Penny, H. A., S. H. Hodge, and M. R. Hepworth. 2018. Orchestration of intestinal homeostasis and tolerance by group 3 innate lymphoid cells. *Semin. Immunopathol.* 40: 357–370.
93. Fabre, T., A. M. S. Barron, S. M. Christensen, S. Asano, K. Bound, M. P. Lech, M. H. Wadsworth, 2nd, X. Chen, C. Wang, J. Wang, et al. 2023. Identification of a broadly fibrogenic macrophage subset induced by type 3 inflammation. *Sci. Immunol.* 8: eadd8945.